Morphologic and functional correlates of synaptic pathology in the cathepsin D knockout mouse model of congenital neuronal ceroid lipofuscinosis

Published in final edited form as:
J Neuropathol Exp Neurol. 2011 December ; 70(12): 1089–1096. doi:10.1097/NEN.0b013e318238fc28.

Morphological and Functional Correlates of Synaptic Pathology in the Cathepsin D Knock-Out Mouse Model of Congenital Neuronal Ceroid-Lipofuscinosis

Sabine Koch, PhD[1], **Svetlana M. Molchanova, PhD**[1], **Ann K Wright, HNC**[2], **Andrew Edwards, MRes**[2], **Jon D. Cooper, PhD**[3], **Tomi Taira, PhD**[1], **Thomas H. Gillingwater, PhD**[2], and **Jaana Tyynelä, PhD**[1]

[1]Institute of Biomedicine/Biochemistry and Neuroscience Center and Department of Biosciences and Department of Veterinary Biosciences, University of Helsinki, Helsinki, Finland [2]Euan MacDonald Centre for Motor Neurone Disease Research & Centre for Integrative Physiology, University of Edinburgh, Edinburgh, UK [3]Department of Neuroscience, MRC Centre for Neurodegeneration Research, Institute of Psychiatry, King's College, London, UK.

Abstract

Mutations in the cathepsin D (CTSD) gene cause an aggressive neurodegenerative disease (congenital neuronal ceroid lipofuscinosis) that leads to early death. Recent evidence suggests that presynaptic abnormalities play a major role in the pathogenesis of CTSD deficiencies. To identify the early events that lead to synaptic alterations, we investigated synaptic ultrastructure and function in pre-symptomatic CTSD knock-out (*Ctsd*$^{-/-}$) mice. Electron microscopy revealed that there were significantly greater numbers of readily releasable synaptic vesicles present in *Ctsd*$^{-/-}$ mice than in wild-type control mice as early as postnatal day 16. The size of this synaptic vesicle pool continued to increase with disease progression in the hippocampus and thalamus of the *Ctsd*$^{-/-}$ mice. Electrophysiology revealed a markedly decreased frequency of miniature excitatory postsynaptic currents (EPSCs) with no effect on pair-pulse modulation of the evoked EPSPs in the hippocampus of *Ctsd*$^{-/-}$ mice. The reduced miniature EPSC frequency was observed before the appearance of epilepsy or any morphological sign of synaptic degeneration. Taken together, the data indicate that CTSD is required for normal synaptic function, and that a failure in synaptic trafficking or recycling may be an early and important pathological mechanism in *Ctsd*$^{-/-}$ mice; these presynaptic abnormalities may initiate synaptic degeneration in advance of subsequent neuronal loss.

Keywords

Cathepsin D; Electron microscopy; Electrophysiology; Hippocampus; Synapse; Synaptic vesicle

Send correspondence and reprint requests to: Jana Tyynelä, PhD, University of Helsinki, Institute of Biomedicine/Biochemistry and Neuroscience Center and Department of Biosciences and Department of Veterinary Biosciences, Haartmanink 8, Helsinki, 00290, Finland. Tel: +358-9-191 25431; Fax: +358-9-191 25444; jaana.tyynela@helsinki.fi.

Europe PMC Funders Author Manuscripts

INTRODUCTION

Cathepsin D (CTSD) deficiency causes a devastating inherited neurological disease in humans, known as congenital neuronal ceroid-lipofuscinosis (cNCL, also called CLN10; MIM #610127) (1). Affected babies have epilepsy, extreme brain atrophy, and die from cardiac failure within the first few days of life (1-3). The disease is characterized neuropathologically by profound loss of neurons and myelin, together with pronounced glial activation throughout the neocortex (1-3). CTSD deficiency also occurs in sheep, in which it causes a congenital disease with neonatal death, and in American bulldogs, in which the disease has a more prolonged course (4, 5). In addition, models of CTSD deficiency have been created in *Drosophila* and mice by genetic modification (6, 7).

Ctsd knock-out (*Ctsd*$^{-/-}$) mice, generated by gene targeting, provide an excellent tool for studying the basic pathophysiology of cNCL (7). CTSD-deficient mice appear phenotypically normal at birth, but develop a rapidly progressive neurodegenerative disease with epileptic seizures and death at postnatal day (P) 26 ± 2 (7-9). Many of the neuropathological features typical of human cNCL are recapitulated in *Ctsd*$^{-/-}$ mice, including accumulation of electron dense storage material in neurons, extensive glial activation, dysmyelination and loss of neurons (8, 10-11).

Recent data from *Ctsd*$^{-/-}$ mice, and from mice that model other forms of NCL (12-15), suggest that early synaptic alterations are characteristic of these disorders. In *Ctsd*$^{-/-}$ mice, synaptic pathology was particularly prevalent in the somatosensory cortex and the related thalamic nuclei (ventral posteromedial and ventral posterolateral nuclei, VPM/VPL); the synaptic density in these areas is also reduced at late-symptomatic stages of disease (10). Loss of synapses was accompanied by aggregation of pre-synaptic proteins, including α-synuclein and SNARE proteins (10, 16). Similar pathological alterations at the synapse have been noted in autopsy samples from CTSD-deficient patients (unpublished observation), indicating that presynaptic mechanisms play an important role in the pathogenesis of CTSD deficiencies.

In this study, we have undertaken a correlated ultrastructural and functional analysis of hippocampal synapses from *Ctsd*$^{-/-}$ mice to investigate the early events that may underlie synaptic pathology. We identified morphological and functional changes that occur in synapses of *Ctsd*$^{-/-}$ mice at pre-symptomatic time points. The most notable changes included an increase in the number of docked synaptic vesicles and a decreased frequency of miniature excitatory postsynaptic currents (mEPSCs).

MATERIALS AND METHODS

Animals

Ctsd$^{-/-}$ mice (7) were maintained on a mixed C57BL6J strain background at the animal facility of the Helsinki University, Biomedicum, where food and water were available ad libitum and with 12 hour/12 hour light/dark cycle. The study protocol was approved by the local Ethical Committee.

Electron Microscopy

P16 and P24 *Ctsd*$^{-/-}$ mice and wild-type (wt) littermate controls were transcardially perfused with 4% paraformaldehyde. Brains were prepared for ultrastructural analysis of synapses, as previously described (17). Briefly, brains were sectioned coronally at 70 μm on a vibratome before post-fixation in 1% osmium tetroxide solution for 45 minutes. Sections were dehydrated using a descending series of alcohols and stained en-bloc using 1% uranyl acetate. Sections were mounted in Durcupan resin (Sigma, Gillingham, UK) on glass slides.

VPM/VPL thalamic nuclei and the CA1 region of the hippocampus were microdissected and mounted on Durcupan resin blocks. Ultra-thin sections (~70 nm thick) were then cut and stained with lead citrate before viewing on a Philips CM12 Transmission Electron Microscope equipped with a Gatan digital camera.

Electron micrographs were analyzed and quantified using ImageJ software. One hundred randomly selected micrographs were analyzed per mouse, with the investigator blind to the age and genotype of the tissue. Only synapses the profiles of which were contained entirely within the micrograph or those crossing the top or left borders of the micrograph were counted. The vast majority (>98%) of synapses had typical excitatory, asymmetric morphology but symmetric synapses were also included in the counts when they ere observed. Pre-synaptic bouton areas were measured by the investigator manually defining the boundaries of each bouton using standard functions within the ImageJ software. Synaptic vesicles were identified by their ~50-nm size. Docked synaptic vesicles were classified as being within 100 nm of the pre-synaptic membrane directly opposing the post-synaptic density. A minimum of 50 individual synapses was assessed per mouse.

Preparation of Acute Slices

P16–P18 *Ctsd*$^{-/-}$ and wt littermate mice (P0 = day of birth) were rapidly killed by decapitation in accordance with the University of Helsinki animal welfare guidelines. Hippocampal slices (400 μm thick) were cut with a vibratome using standard methods (18). The slices were used 1 to 4 hours after cutting.

Electrophysiology

For electrophysiological recordings, the slices were placed in a submerged chamber and superfused with artificial cerebrospinal fluid containing (mM): 124 NaCl, 3 KCl, 1.25 NaH_2PO_4, 1 $MgSO_4$, 26 $NaHCO_3$, 15 d-glucose and 2 $CaCl_2$; 5% CO_2–95% O_2, at a rate of 2–3 ml minute^{-1} (32°C). Whole-cell recordings were obtained from CA1 pyramidal neurons using the Axopatch 200B amplifier (Axon Instruments, Union City, CA). Cells were voltage-clamped at −70 mV with 3 to 5 MΩ pipettes filled with a solution containing (mm): 130 $CsMeSO_4$, 10 Hepes, 0,5 EGTA, 4 Mg-ATP, 0.3 Na-GTP, 5 *N*-(2,6-dimethylphenylcarbamoylmethyl) triethylammonium chloride and 8 NaCl (285 mOsm), pH 7.2. AMPA-receptor-mediated mEPSCs (mEPSCs) were recorded from CA1 pyramidal neurons in the presence of antagonists of GABAA and voltage-dependent sodium channels (picrotoxin [100 μM] and TTX [1 μM], respectively). To measure the paired pulse facilitation, the pipette filling solution was changed (mM): 115 $CsMeSO_4$, 10 Hepes, 10 EGTA, 4 Mg-ATP, 0.3 Na-GTP, 5 *N*-(2,6-dimethylphenylcarbamoylmethyl) triethylammonium chloride and 8 NaCl (285 mOsm), pH 7.2. A bipolar electrode was used for afferent stimulation. EPSCs were evoked by stimulation of Schaffer collateral-commissural fibers and recorded from CA1 pyramidal neurons in the presence of GABA-A and NMDAR antagonists (100 μM picrotoxin and 50 μM AP5, respectively). All compounds were from Tocris (Bristol, UK).

WinLTP (0.95b or 0.96, www.winltp.com, (19) or Axoscope 9.2 (Axon Instruments) was used for data acquisition. Offline analysis was performed using WinLTP or MiniAnalysis 6.0.3 program (Synaptosoft Inc, Decatur, GA). Spontaneous events were detected using peak detector algorithm, and all events were confirmed visually. The cumulative distributions of mEPSCs were constructed from at least 10 minutes of recording (at least 50 events) from each cell, using a bin width of 100 ms for inter-event interval and 1 pA for amplitude. The pooled data are given as mean ± SEM for the number of cells indicated. Student two-tailed t-test was used for statistical analysis. The level of significance was set as $p < 0.05$.

RESULTS

Synaptic Density Is Markedly Decreased in the Hippocampus and Thalamus of late-Symptomatic *Ctsd*$^{-/-}$ Mice

Our previous semiquantitative analyses revealed reduced numbers of synapses in the VPM/VPL thalamic nuclei of *Ctsd*$^{-/-}$ mice at P24 (10). We validated these findings using a more robust quantitative method, confirming a significant loss of synapses at P24 (***$p < 0.001$; ANOVA with Tukey's post-hoc test; Fig. 1A). A similar analysis at pre-symptomatic age (P16) revealed a clear, but not statistically significant, reduction in synaptic density in VPM/VPL ($p > 0.05$; Fig. 1A), indicating that synaptic pathology was only in its early stages at P16.

Because assessing synaptic function using electrophysiological methods in VPM/VPL is difficult, we extended our experiments to determine whether synapses in the hippocampus (a region ideal for electrophysiological experiments) were also affected. Synaptic density remained unchanged in the CA1 region of hippocampus at P16, but was significantly reduced at P24 (**$p < 0.01$; Fig. 1B). However, the magnitude of synapse loss in the hippocampus (~60% reduction) was not as large as that observed in the VPM/VPL (~90% reduction). Nevertheless these data (together with established protocols for slice preparation and electrophysiological recordings) suggest that the hippocampus provides an appropriate brain region for correlated ultrastructural and functional analyses of synapses in *Ctsd*$^{-/-}$ mice. Moreover, the data indicate that P16 represents a time point at which synaptic degeneration has not yet begun in the hippocampus, whereas P24 represents a time point when there is extensive synaptic degeneration.

Synaptic Vesicle Density Is Increased in *Ctsd*$^{-/-}$ Mice

Qualitative observations of synapses in the hippocampal CA1 region from *Ctsd*$^{-/-}$ mice suggested that there was no obvious change in the size of synaptic boutons at either pre- or late-symptomatic time points (Fig. 2A, B). Quantitative analyses confirmed these observations (Fig. 2C). However, synaptic vesicle pools appeared to be changed qualitatively in CA1 synapses at both pre- and late-symptomatic time points, i.e. denser clustering of vesicles around pre-synaptic membranes was routinely observed at P24 in *Ctsd*$^{-/-}$ mice (Fig. 2B). Quantitative analysis of total synaptic vesicle densities in CA1 showed no difference between genotypes at P16, but at P24 there was a significant increase in *Ctsd*$^{-/-}$ mice (*$p < 0.05$; ANOVA with Tukey's post-hoc test; Fig. 2D). Most strikingly, however, the number of docked vesicles was significantly increased in CA1 synapses from *Ctsd*$^{-/-}$ mice, with significant changes already present at P16 ($p < 0.05$; Fig. 2E). The number of docked vesicles was almost double that in control mice by P24 ($P < 0.05$; Fig. 2E). Although not statistically significant, a similar trend was observed for the numbers of undocked vesicles in these mutant mice (Fig. 2F). These data indicate that disruption of hippocampal synaptic vesicle localization and/or recycling is an early pathological event in *Ctsd*$^{-/-}$ mice.

To determine whether the changes observed in synaptic vesicle densities in CA1 were a common feature of synaptic pathology in *Ctsd*$^{-/-}$ mice, we quantified synaptic vesicle densities in VPM/VPL at P16 and P24 (Fig. 3A, B). The number of docked synaptic vesicles and the total number of vesicles in VPM/VPL were significantly increased (**$p < 0.01$; ***$p < 0.001$; Fig. 3C, D) at P24, but not at P16.

mEPSC Frequency Is Decreased in *Ctsd*$^{-/-}$ Mice

To determine the functional effects of the increased numbers of docked synaptic vesicles in the hippocampal CA1 region of *Ctsd*$^{-/-}$ mice, pharmacologically isolated AMPA mEPSCs

were recorded from hippocampal pyramidal cells in the CA1 subfield (Fig. 4A-D). At P16-P18 there was a lower mEPSC frequency in *Ctsd*$^{-/-}$ mice vs. controls. The mEPSC inter-event interval in the mutants was about twice as long as in wild-type mice (wt: 2.74 ± 0.31 seconds; *Ctsd*$^{-/-}$: 5.89 ± 1.17 seconds; $p < 0.05$; Fig. 4E). There was, however, no difference between genotypes in the AMPA mEPSC amplitude (wt: 14.04 ± 0.80 pA; *Ctsd*$^{-/-}$: 14.48 ± 0.99 pA; $p > 0.05$; Fig. 4F).

Release Probability Is Unaltered in *Ctsd*$^{-/-}$ Mice

Because an increased number of docked synaptic vesicles may be associated with increased neurotransmitter release (20), we next measured paired-pulse facilitation (PPF) in the CA3-CA1 synapse because it is inversely correlated with a change in the initial release probability (P_r) (20, 22, 23). To assess PPF we used inter-pulse intervals of 20 ms (50 Hz), 50 ms (20 Hz) and 150 ms (6, 7 Hz). We found no difference in PPF between the genotypes at any of the inter-pulse intervals used (pair-pulse ratio, 20-ms-interval: wt 2.54 ± 0.08, *Ctsd*$^{-/-}$ 2.61 ± 0.19; 50-ms-interval: wt 2.13 ± 0.14, *Ctsd*$^{-/-}$ 2.17 ± 0.22; 150-ms-interval: wt 1.50 ± 0.05, *Ctsd*$^{-/-}$ 1.27 ± 0.19; $p > 0.05$; Fig. 5), indicating that the release probability is unaltered in *Ctsd*$^{-/-}$ mice.

DISCUSSION

Readily Releasable Synaptic Vesicle Pool Size Increases with Disease Progression in *Ctsd*$^{-/-}$ Mice

Our most important ultrastructural finding in the synapses of *Ctsd*$^{-/-}$ mice was a marked increase in vesicle pool size compared to controls. Indeed, the readily releasable synaptic vesicle pool size was already significantly increased (~1.2-fold) in hippocampal neurons of *Ctsd*$^{-/-}$ mice at P16, which represents a pre-symptomatic stage of the disease. If there were a significant loss of synapses at P16, an increased number of synaptic vesicles could reflect a compensatory mechanism as a response to synaptic loss. However, at this stage, synaptic loss was not yet evident in CA1 of these affected mice. By P24, the size of the readily releasable vesicle pool had increased markedly, not only in the CA1 (~1.7-fold) but also in the thalamus (~1.5-fold). In addition, the total number of synaptic vesicles per bouton was significantly increased in both of these brain regions, suggesting that the synaptic vesicle pool undergoes abnormal changes throughout the brain of *Ctsd*$^{-/-}$ mice. Inasmuch as the changes in the vesicle pool size occurred in advance of synaptic degeneration in the hippocampus of *Ctsd*$^{-/-}$ mice, the data raise the possibility that alterations in synaptic vesicle recycling may contribute to the initiation and progression of synaptic degeneration in these mice. These findings are in line with our previously reported alterations in the distribution of presynaptic proteins in *Ctsd*$^{-/-}$ mice (10).

Electrophysiological Data Indicate Early Dysfunction of Synapses in *Ctsd*$^{-/-}$ Mice

The synaptic vesicle pool size and, particularly, the number of readily releasable synaptic vesicles (so called “docked” vesicles) affect the efficacy of synaptic transmission (20). The increased number of docked vesicles may lead to an increased neurotransmitter release and to a consequent increase in postsynaptic currents (20, 22-23). Somewhat surprisingly, our observations contradict this principle, i.e. despite the increased number of docked vesicles in *Ctsd*$^{-/-}$ mice, the paired-pulse data suggested no change in the P_{r-}. Rather, the increased number of readily releasable vesicles was associated with a lower frequency of AMPA-mediated mEPSCs. The lower mEPSC frequency might be explained by the presence of synaptic degeneration and loss, which would not necessarily alter the overall P_r in these synapses. Although we found no morphological evidence for synaptic loss in the CA1 of *Ctsd*$^{-/-}$ mice at P16, it is reasonable to suggest that the reduced mEPSC frequency was likely caused by changes in the functional parameters of synapses before they underwent

morphologically visible degeneration. In previous electrophysiological analyses, spontaneous burst discharges of an epileptiform nature were recorded from the hippocampus of *Ctsd*$^{-/-}$ mice at late-symptomatic ages (P24) (8, 21), but were not observed at P16 (21). This suggests that the synaptic dysfunction reported in the present study precedes the onset of epilepsy and synaptic degeneration in *Ctsd*$^{-/-}$mice.

Comparison with Other Forms of NCL

The NCLs are a genetically heterogenous group of fatal neurodegenerative diseases, sharing common clinical symptoms and pathological events (24, 25). The existence of several diverse mouse models of NCL allows comparison of the basic mechanisms underlying the diseases (24-25). In contrast to our findings in *Ctsd*$^{-/-}$ mice, the size of the readily releasable synaptic vesicle pool has been shown to progressively decline in cultured neurons of palmityl-protein thioesterase 1 (*Ppt1*) knock-out mice, a model of infantile NCL disease (12). This reduction was associated with decreased frequency of spontaneous mEPSCs (12). Whether the differences observed between this study and ours reflect different roles of PPT1 and CTSD in regulating synaptic vesicle dynamics, or whether other factors affected the results (e.g. comparing in vitro changes with in vivo pathology) remains unclear. The major neuropathological changes in *Ppt1* knock-out mice closely resemble those in *Ctsd*$^{-/-}$ mice, with synaptic pathology occurring in a regionally selective manner, preceding the onset of neuronal loss in the thalamus and cortex (10, 15). Similar pathological changes are evident in autopsy material of infantile NCL patients with PPT1 deficiency and it has been suggested that the lack of PPT1 activity leads to altered synaptic vesicle trafficking at nerve terminals (14). Thus, whatever the basis for these events, it is becoming apparent that the presynaptic compartment is targeted early in the pathogenesis of the NCLs. Although the precise nature of the early events underlying synaptic pathology may differ between the forms of NCL, invariably these changes lead to synapse degeneration and subsequent neuronal loss.

Decreased frequency of spontaneous mEPSCs at an early age has only been reported in a few mouse models. These models have genetic defects affecting elementary functions of the brain and/or causing severe neurological diseases, such as neocortical maturation and autism (26), frontotemporal dementia (27), and Huntington disease (28). The early appearance of functional alterations in the synapses of *Ctsd*$^{-/-}$ mice suggests that CTSD has a fundamental role in maintenance and perhaps even development of synapses and neuronal networks. This possibility is supported by our previous findings showing that the somatosensory thalamocortical system is a focus of major pathological alterations in these mice (10). The abnormal accumulation of synaptic vesicles in *Ctsd*$^{-/-}$ brains indicates that the function of CTSD may be related to recycling or trafficking of presynaptic vesicles.

Relationship to Other “Synaptopathies”

In the most common forms of age-related dementia, such as Alzheimer disease and Parkinson disease, the role of synaptic loss in the neurodegenerative process has been recognized since the early 1990s (29, 30). Subsequently, there has been growing evidence of early synaptic vulnerability in a number of different neurodegenerative conditions affecting both central and peripheral nervous systems, including Alzheimer and Huntington disease, prion diseases, and spinal muscular atrophy (31-36). In particular, disruption of synaptic functions may precede synaptic degeneration and loss in many of these diseases (31-34), whereas the exact functional mechanisms may vary from one disease to another.

Summary

We have quantitatively assessed synaptic pathology in the thalamus and hippocampus of *Ctsd*$^{-/-}$ mice at an ultrastructural and functional level. We observed a significant increase in

the number of docked vesicles at individual synapses occurring in advance of synaptic degeneration and neuron loss. These structural changes were accompanied by a markedly decreased frequency of mEPSCs, but no effects on evoked excitatory post-synaptic potentials. Taken together, the present data provide the first direct evidence for functional and structural changes at the synapse in pre-symptomatic *Ctsd*$^{-/-}$ mice and strongly suggest that a failure in the presynaptic function initiates synaptic degeneration, which leads to neuronal degeneration in these mice. These findings further emphasize the role of CTSD in maintaining synaptic integrity in vivo.

Acknowledgments

Support: Academy of Finland (JT), BDSRA and the Wellcome Trust (THG and JDC), Batten Disease Family Association and The Natalie Fund (JDC), Academy of Finland and Sigrid Juselius Foundation (SM and TT).

REFERENCES

1. Siintola E, Partanen S, Strömme P, et al. Cathepsin D deficiency underlies congenital human neuronal ceroid-lipofuscinosis. Brain. 2006; 129:1438–45. [PubMed: 16670177]
2. Garborg I, Torvik A, Hals J, et al. Congenital neuronal ceroid lipofuscinosis. A case report. Acta Pathol Microbiol Immunol Scand A. 1987; 95:119–25. [PubMed: 3604683]
3. Fritchie K, Siintola E, Armao D, et al. Novel mutation and the first prenatal screening of cathepsin D deficiency (CLN10). Acta Neuropathol. 2009; 117:201–8. [PubMed: 18762956]
4. Tyynelä J, Sohar I, Sleat DE, et al. A mutation in the ovine cathepsin D gene causes a congenital lysosomal storage disease with profound neurodegeneration. EMBO J. 2000; 19:2786–92. [PubMed: 10856224]
5. Awano T, Katz ML, O'Brien DP, et al. A mutation in the cathepsin D gene (CTSD) in American Bulldogs with neuronal ceroid lipofuscinosis. Mol Genet Metab. 2006; 87:341–8. [PubMed: 16386934]
6. Myllykangas L, Tyynelä J, Page-McCaw A, et al. Cathepsin D-deficient Drosophila recapitulate the key features of neuronal ceroid lipofuscinoses. Neurobiol Dis. 2005; 19:194–9. [PubMed: 15837574]
7. Saftig P, Hetman M, Schmahl W, et al. Mice deficient for the lysosomal proteinase cathepsin D exhibit progressive atrophy of the intestinal mucosa and profound destruction of lymphoid cells. EMBO J. 1995; 14:3599–608. [PubMed: 7641679]
8. Koike M, Nakanishi H, Saftig P, et al. Cathepsin D deficiency induces lysosomal storage with ceroid lipofuscin in mouse CNS neurons. J Neurosci. 2000; 20:6898–906. [PubMed: 10995834]
9. Haapanen A, Ramadan UA, Autti T, et al. In vivo MRI reveals the dynamics of pathological changes in the brains of cathepsin D-deficient mice and correlates changes in manganese-enhanced MRI with microglial activation. Magn Reson Imaging. 2007; 25:1024–31. [PubMed: 17451907]
10. Partanen S, Haapanen A, Kielar C, et al. Synaptic changes in the thalamocortical system of cathepsin D-deficient mice: a model of human congenital neuronal ceroid-lipofuscinosis. J Neuropathol Exp Neurol. 2008; 67:16–29. [PubMed: 18091563]
11. Mutka AL, Haapanen A, Käkelä R, et al. Murine cathepsin D deficiency is associated with dysmyelination/myelin disruption and accumulation of cholesteryl esters in the brain. J Neurochem. 2010; 112:193–203. [PubMed: 19845830]
12. Virmani T, Gupta P, Liu X, et al. Progressively reduced synaptic vesicle pool size in cultured neurons derived from neuronal ceroid lipofuscinosis-1 knockout mice. Neurobiol Dis. 2005; 20:314–23. [PubMed: 16242638]
13. Wishart TM, Parson SH, Gillingwater TH. Synaptic vulnerability in neurodegenerative disease. J Neuropathol Exp Neurol. 2006; 65:733–9. [PubMed: 16896307]
14. Kim SJ, Zhang Z, Sarkar C, et al. Palmitoyl protein thioesterase-1 deficiency impairs synaptic vesicle recycling at nerve terminals, contributing to neuropathology in humans and mice. J Clin Invest. 2008; 118:3075–86. [PubMed: 18704195]

15. Kielar C, Wishart TM, Palmer A, et al. Molecular correlates of axonal and synaptic pathology in mouse models of Batten disease. Hum Mol Genet. 2009; 18:4066–80. [PubMed: 19640925]
16. Cullen V, Lindfors M, Ng J, et al. Cathepsin D expression level affects alpha-synuclein processing, aggregation, and toxicity in vivo. Mol Brain. 2009; 2:5. [PubMed: 19203374]
17. Gillingwater TH, Ingham CA, Parry KE, et al. Delayed synaptic degeneration in the CNS of Wlds mice after cortical lesion. Brain. 2006; 129:1546–56. [PubMed: 16738060]
18. Lauri SE, Vesikansa A, Segerstråle M, et al. Functional maturation of CA1 synapses involves activity-dependent loss of tonic kainate receptor-mediated inhibition of glutamate release. Neuron. 2006; 50:415–29. [PubMed: 16675396]
19. Anderson WW, Collingridge GL. Capabilities of the WinLTP data acquisition program extending beyond basic LTP experimental functions. J Neurosci Methods. 2007; 162:346–56. [PubMed: 17306885]
20. Zucker RS, Regehr WG. Short-term synaptic plasticity. Annu Rev Physiol. 2002; 64:355–405. [PubMed: 11826273]
21. Shimizu T, Hayashi Y, Yamasaki R, et al. Proteolytic degradation of glutamate decarboxylase mediates disinhibition of hippocampal CA3 pyramidal cells in cathepsin D-deficient mice. J Neurochem. 2005; 94:680–90. [PubMed: 15992379]
22. Dobrunz LE, Stevens CF. Heterogeneity of release probability, facilitation, and depletion at central synapses. Neuron. 1997; 18:995–1008. [PubMed: 9208866]
23. Dobrunz LE. Release probability is regulated by the size of the readily releasable vesicle pool at excitatory synapses in hippocampus. Int J Dev Neurosci. 2002; 20:225–36. [PubMed: 12175858]
24. Jalanko A, Braulke T. Neuronal ceroid lipofuscinoses. Biochim Biophys Acta. 2009; 1793:697–709. [PubMed: 19084560]
25. Kohlschütter A, Schulz A. Towards understanding the neuronal ceroid lipofuscinoses. Brain Dev. 2009; 31:499–502. [PubMed: 19195801]
26. Yashiro K, Riday TT, Condon KH, et al. Ube3a is required for experience-dependent maturation of the neocortex. Nat Neurosci. 2009; 12:777–83. [PubMed: 19430469]
27. Belly A, Bodon G, Blot B, et al. CHMP2B mutants linked to frontotemporal dementia impair maturation of dendritic spines. J Cell Sci. 2010; 1:2943–5. [PubMed: 20699355]
28. Cepeda C, Hurst RS, Calvert CR, et al. Transient and progressive electrophysiological alterations in the corticostriatal pathway in a mouse model of Huntington's disease. J Neurosci. 2003; 23:961–9. [PubMed: 12574425]
29. Terry RD, Masliah E, Salmon DP, et al. Physical basis of cognitive alterations in Alzheimer's disease: synapse loss is the major correlate of cognitive impairment. Ann Neurol. 1991; 30:572–80. [PubMed: 1789684]
30. Sauer H, Oertel WH. Progressive degeneration of nigrostriatal dopamine neurons following intrastriatal terminal lesions with 6-hydroxydopamine: a combined retrograde tracing and immunocytochemical study in the rat. Neuroscience. 1994; 59:401–15. [PubMed: 7516500]
31. Chapman PF, White GL, Jones MW, et al. Impaired synaptic plasticity and learning in aged amyloid precursor protein transgenic mice. Nat Neurosci. 1999; 2:271–6. [PubMed: 10195221]
32. Jeffrey M, Halliday WG, Bell J, et al. Synapse loss associated with abnormal PrP precedes neuronal degeneration in the scrapie-infected murine hippocampus. Neuropathol Appl Neurobiol. 2000; 26:41–54. [PubMed: 10736066]
33. Klapstein GJ, Fisher RS, Zanjani H, et al. Electrophysiological and morphological changes in striatal spiny neurons in R6/2 Huntington's disease transgenic mice. J Neurophysiol. 2001; 86:2667–77. [PubMed: 11731527]
34. Coleman P, Federoff H, Kurlan R. A focus on the synapse for neuroprotection in Alzheimer disease and other dementias. Neurology. 2004; 63:1155–62. [PubMed: 15477531]
35. DiProspero NA, Chen EY, Charles V, et al. Early changes in Huntington's disease patient brains involve alterations in cytoskeletal and synaptic elements. J Neurocytol. 2004; 33:517–33. [PubMed: 15906159]
36. Murray LM, Comley LH, Thomson D, et al. Selective vulnerability of motor neurons and dissociation of pre- and post-synaptic pathology at the neuromuscular junction in mouse models of spinal muscular atrophy. Hum Mol Genet. 2008; 17:949–62. [PubMed: 18065780]

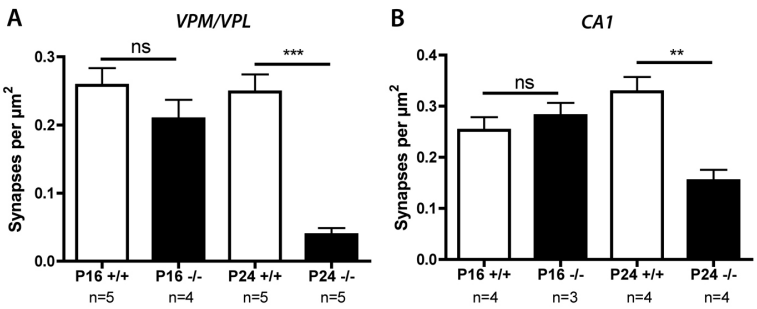

Figure 1.

Synaptic density in the ventral posteromedial and ventral posterolateral nuclei (VPM/VPL) nuclei of the thalamus and the CA1 region of hippocampus in *Ctsd*$^{-/-}$ and control mice. (**A**) Bar chart (mean ± SEM) showing synaptic density in the VPM/VPL nuclei quantified from electron micrographs from *Ctsd*$^{-/-}$ mice (−/−; black bars) and control mice (+/+; white bars). There is a subtle reduction in the number of synapses at postnatal day (P) 16 (pre-symptomatic; not significant $p > 0.05$) and a significant loss of synapses by P24 (late-symptomatic; *** $p < 0.001$). (**B**) Bar chart showing synaptic density in the CA1 region of hippocampus quantified from electron micrographs. There was no reduction in the number of synapses at P16 (pre-symptomatic; not significant $p > 0.05$), but there was a significant loss of synapses by P24 (late-symptomatic; ** $p < 0.01$). n = number of mice per genotype/age.

Europe PMC Funders Author Manuscripts

Europe PMC Funders Author Manuscripts

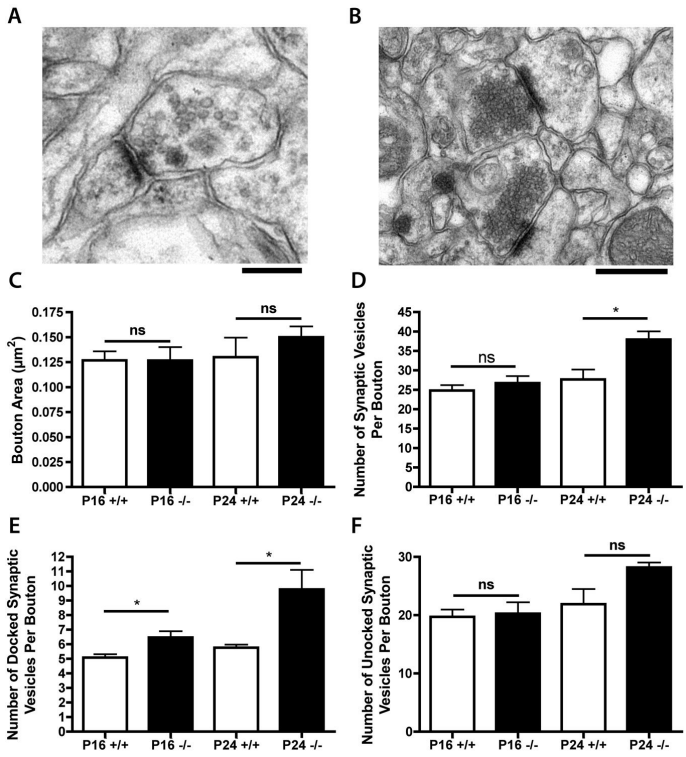

Figure 2.

Synaptic vesicle pools in the CA1 region of hippocampus in *Ctsd*$^{-/-}$ and control mice. (**A, B**) Representative electron micrographs showing synapses in the CA1 of control (**A**) and *Ctsd*$^{-/-}$ (**B**) mice at postnatal day (P) 24. Note the clustering of synaptic vesicles towards the pre-synaptic membrane in the *Ctsd*$^{-/-}$ synapses (**B**). (**C**) Bar chart (mean ± SEM) showing synaptic bouton areas in CA1 quantified from electron micrographs of *Ctsd*$^{-/-}$ (−/−; black bars) and wild-type control mice (+/+; white bars). (**D**) Bar chart showing synaptic vesicle densities in CA1, revealing a significant increase in *Ctsd*$^{-/-}$ mice at P24 (* $p < 0.05$). (**E**) Bar chart showing average numbers of docked synaptic vesicles per synapse in CA1, revealing a significant increase in *Ctsd*$^{-/-}$ mice at pre-symptomatic (P16) and late-symptomatic (P24) time points (* $p < 0.05$). (**F**) Bar chart showing average numbers of undocked synaptic vesicles per synapse in CA1. See Figure 1 for the number of mice in each group.

Europe PMC Funders Author Manuscripts

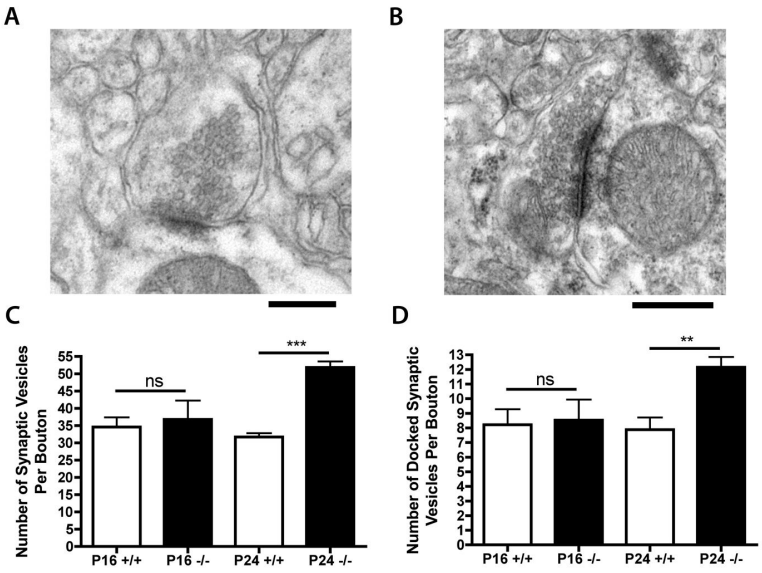

Figure 3.

Synaptic vesicle pools in synapses from ventral posteromedial and ventral posterolateral thalamic nuclei (VPM/VPL) nuclei of *Ctsd*$^{-/-}$ and control mice. (**A, B**) Representative electron micrographs showing synapses in the VPM/VPL of control (**A**) and *Ctsd*$^{-/-}$ (**B**) mice at postnatal day (P) 24. Note the clustering of synaptic vesicles towards the pre-synaptic membrane in the *Ctsd*$^{-/-}$ synapses (**B**). (**C**) Bar chart (mean ± SEM) showing synaptic vesicle densities in the VPM/VPL, revealing a significant increase in *Ctsd*$^{-/-}$ mice (−/−; black bars) at P24 compared to control mice (+/+; white bars; *** $p < 0.001$). (**D**) Bar chart showing average numbers of docked synaptic vesicles per synapse in the VPM/VPL, revealing a significant increase in *Ctsd*$^{-/-}$ mice at P24 (** $p < 0.01$). See Figure 1 for the number of mice in each group.

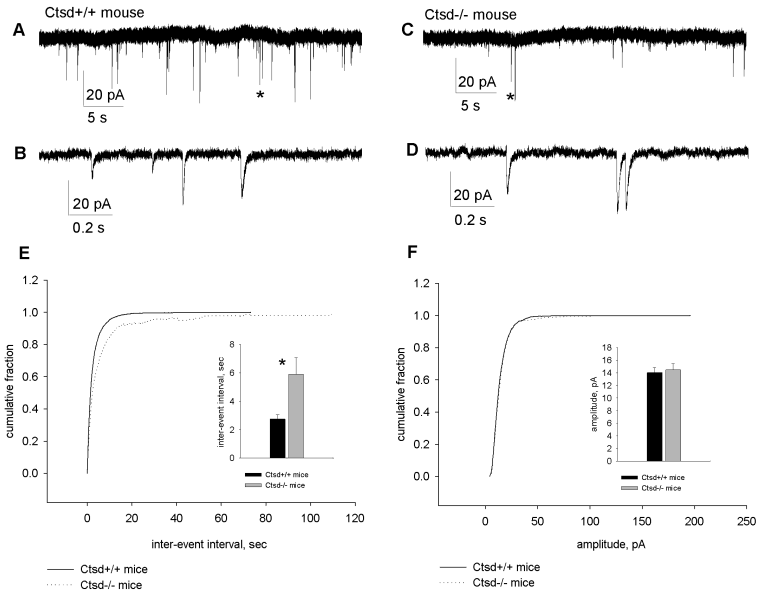

Figure 4.

(A-D) Characteristics of miniature excitatory postsynaptic currents (EPSCs) recorded from hippocampal CA1 pyramidal neurons of wild-type (**A, B**) and *Ctsd*$^{-/-}$ mice (**C, D**) at postnatal day (P) 16-17. Asterisks in example recordings (**A, C**) indicate regions presented with the expanded time scale (**B, D**). (**E**) Cumulative distribution and averaged values of mEPSC inter-event interval, * $p < 0.05$. (**F**) The cumulative distribution and averaged values of mEPSC amplitude.

Europe PMC Funders Author Manuscripts

Europe PMC Funders Author Manuscripts

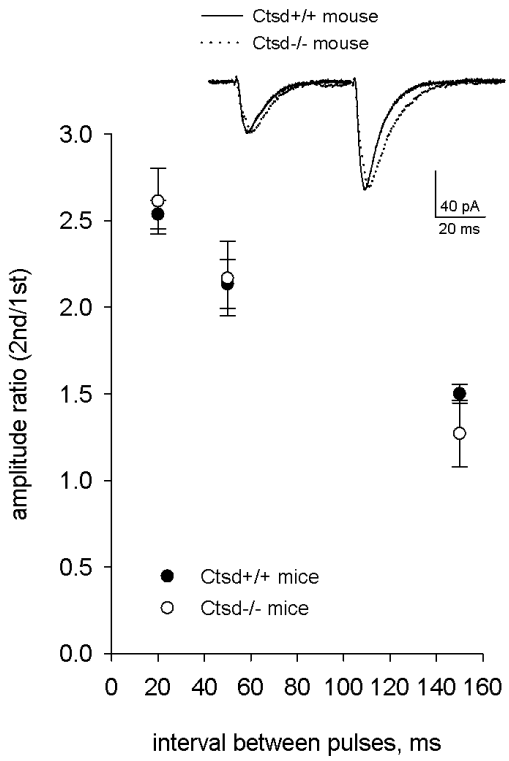

Figure 5.

Characteristics of synaptic responses evoked by stimulation of Shaffer collateral and recorded from hippocampal CA1 pyramidal neurons of wild-type and *Ctsd*$^{-/-}$ mice. Mean values of amplitude paired-pulse ratio recorded with 20-, 50- and 150-ms-interval. Inset: example response at 50-ms-interval (averages of 10 sweeps, normalized by the amplitude of the first peak.